Random walks on jammed networks: Spectral properties

Jeremy B. Lechman,* Stephen D. Bond, Dan S. Bolintineanu, Gary S. Grest, and Cole D. Yarrington
Sandia National Laboratories, Albuquerque, New Mexico 87185, USA

Leonardo E. Silbert
School of Math, Science and Engineering, Central New Mexico Community College, Albuquerque, New Mexico 87106, USA

(Received 8 November 2018; published 15 July 2019)

Using random walk analyses we explore diffusive transport on networks obtained from contacts between isotropically compressed, monodisperse, frictionless sphere packings generated over a range of pressures in the vicinity of the jamming transition $p \to 0$. For conductive particles in an insulating medium, conduction is determined by the particle contact network with nodes representing particle centers and edges contacts between particles. The transition rate is not homogeneous, but is distributed inhomogeneously due to the randomness of packing and concomitant disorder of the contact network, e.g., the distribution of the coordination number. A narrow escape time scale is used to write a Markov process for random walks on the particle contact network. This stochastic process is analyzed in terms of spectral density of the random, sparse, Euclidean and real, symmetric, positive, semidefinite transition rate matrix. Results show network structures derived from jammed particles have properties similar to ordered, euclidean lattices but also some unique properties that distinguish them from other structures that are in some sense more homogeneous. In particular, the distribution of eigenvalues of the transition rate matrix follow a power law with spectral dimension 3. However, quantitative details of the statistics of the eigenvectors show subtle differences with homogeneous lattices and allow us to distinguish between topological and geometric sources of disorder in the network.

DOI: 10.1103/PhysRevE.100.012905

I. INTRODUCTION

What is the relationship between the structure of materials and their bulk properties? The question has a long and distinguished history with relevance to various applied problems. For applications such as energy storage (e.g., batteries) and pyrotechnic igniters in pyrotechnically actuated devices (e.g., air bags), among others, particulate materials (powders and granular materials) are critical to the functionality of manufactured devices. For these devices, the question becomes broader: what role does structural disorder—topological and geometrical—resulting from the discreteness of the material and lack of microscopic control in the manufacturing process play in the variability of material properties and how does this property variability relate to the variability of device performance? The practical challenge is to predict and control the behavior of particulate materials so that they can be processed into robust devices with reliable performance. Alternatively, the challenge is to define the feedstock material characteristics and processing routes that lead to better performance, however that is defined. For powders and granular materials, which are far from equilibrium, this amounts to understanding the interplay between the path-dependent metastable structures that can be obtained from various material types and processing routes and transport (thermal, electrical, mechanical) in those structures.

For granular materials, much focus has been given to the question of mechanical properties of random packings (of typically monodisperse, frictionless, spherical particles) as they approach the limit of mechanical stability—the so-called jamming transition. However, the analogous (scalar) problem of conductive (thermal or electrical) transport in particulate materials is also of critical importance for the aforementioned batteries and pyrotechnics. In such applications, one may be concerned with the sensitivity of the bulk material to, e.g., chemical reactions (as in thermal runaway) which impact device performance or failure. Moreover, for disordered materials, device performance or failure is sensitive to local heterogeneities in material structure (e.g., stress concentration near cracks, or thermal "hot spots" in reactive materials). Again, understanding the relationship between material structure and thermomechanical properties related to a given device's performance behavior along with their prediction and control during the manufacturing process is required.

Similarly, the properties of complex networks are of broad interest as they form the fundamental basis for social, biological, and communications relationships. In addition, there are deep connections between these applications and the behavior of complex, disordered materials. Indeed, many studies illustrate the close relationship between so-called reduced-order models of transport in disordered systems and random walks on networks [1–3]. Here we make use of an accurate, semi-analytical approach to develop such a model and deploy it to acquire insight into the fundamental properties of networks formed by the contact topology of random

*jblechm@sandia.gov

close-packed particulate (granular) systems. In the following section we describe the problem and method in detail and relate the approach here to similar ones in solid state and ordered (i.e., homogeneous or regular) lattice systems. Subsequently, we use spectral analysis to analyze average macroscale conductive transport in disordered, jammed networks of grains. Finally, we analyze the statistics of eigenvectors for these disordered systems to glean some insights into the role of local inhomogeneity and offer some concluding remarks.

II. PROBLEM DESCRIPTION AND APPROACH

We consider conduction through isotropically compressed, monodisperse, frictionless jammed spheres created via discrete element method (DEM) simulations [4,5] with an established (de)compression protocol [6]. Multiple disordered packings of jammed mono-sized spheres were generated for a range of packing fractions ϕ above the jamming transition [7]. The contact networks from packings of $N = 10^3$, 10^4, and 10^5 particles form the objects of our study. The uniquely numbered particle centers determine the vertex/node set while contacts between particles give the edge set of the graph representing the network. Isotropic compression, then, establishes the network edge set; providing a particular random embedding of the contact graph in a three-dimensional (3-D), Euclidean space. Two features of the resulting networks should be noted: (i) they are connected since we remove particles that are isolated and are not in contact with others (typically less than 5% of all particles) from consideration as they do not contribute to the contact network; (ii) it is not bipartite. We consider both nonweighted and weighted representations of this network. The former is quantified through the adjacency matrix of the network, and the latter through weighting the elements of that matrix appropriately based on details of local geometric features of the packed spherical particles. All the subsequent analysis in this work is based on modeling conductive transport in particulate materials as a continuous-time random walk processes on these contact networks. Specifically, we are interested in the spectral properties of the conduction matrix, the operator central to this approach. Hence, isotropic compression can be seen as the "manufacturing" or nonequilibrium process which governs the (random) structure which controls the properties of the bulk, particulate material.

We emphasize that we are concerned here with conduction *through* particles seen as grains and not conduction due to lattice vibrations *of* the particles as in solid-state atomic systems. In this sense the particles are viewed as macroscopic objects composed on internal degrees of freedom which account for the conductive processes. An off-lattice random walker approach [8] can then be used to model the internal degrees of freedom and simulate conduction within and between contacting particles as was done in previous work [7]. Here, however, we take a different approach by effectively coarse-graining the off-lattice random walk within particles to a continuous-time Markov process on the contact network of the particle pack leading to a random walk-type model that is nonetheless analogous to solid-state lattice approaches [9]. To accomplish this, two simplifying assumptions made in [7] are noted: (i) walkers are constrained to remain within the particles, meaning, e.g., no heat flux from particle surfaces due to radiation; and (ii) particle contacts are ideal and provide no barrier for walkers to pass through, e.g., no contact resistance. Given this physical description of the system, an analytical expression for the time it takes an off-lattice random walker to leave a particle and enter a contacting neighbor particle can be found in [10]. In general, the time it takes for a random walker to leave a particle and enter a contacting neighbor particle is dependent upon the starting location within the initial particle. Integrating over all starting locations of a walker in the initial sphere, or volume-averaging, removes the spatial dependence. Hence, the pair-wise volume-averaged mean first passage time (MFPT), τ_{ij}, is the narrow-escape time that it takes for a random walker to pass out of an initial sphere, i, into sphere one of its z_i neighbors, j. z_i is the coordination number (vertex degree) of particle i. Note the distribution of z_i is one of the topological features that distinguish the networks considered here from classical homogeneous lattice or regular graph random walks where z_i is constant. Previous work [7], for packs near the jamming point, found that the bulk, effective conductivity, equivalent to the long-time diffusivity of random walkers constrained to walk within the particles, scales as the inverse of a characteristic time $D_\infty \sim 1/t^*$. Accordingly, t^* was identified with the median value, $t_m \sim t^*$, of the distribution over all particles of their total volume-averaged MFPT, $\bar{t}_i = (\Sigma_{j=1}^{z_i} 1/\tau_{ij})^{-1}$, see Fig. 1. In the following, we use τ_{ij} to formulate a master equation for transport on the "jammed" (particle contact) networks. Thus, volume-averaging effectively coarse-grains the off-lattice,

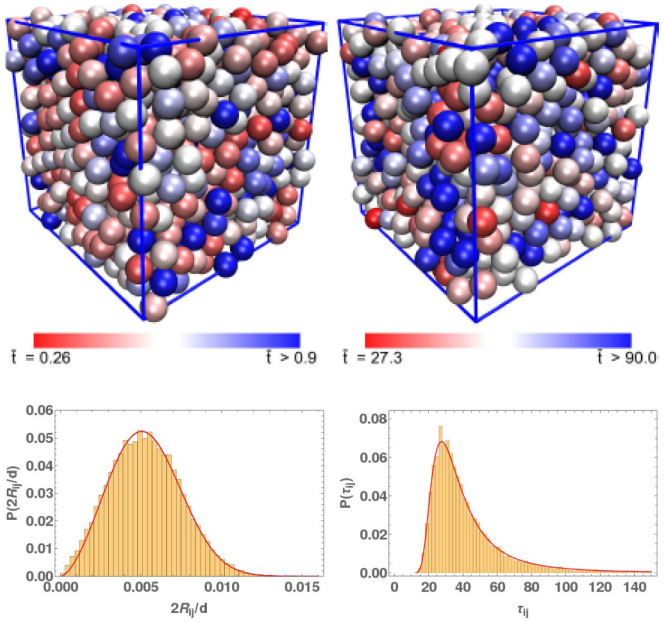

FIG. 1. Top: Disordered, jammed packs of monodisperse, frictionless spheres color coded by total volume-averaged mean first passage time, $\bar{t}_i = (\Sigma_{j=1}^{z_i} 1/\tau_{ij})^{-1}$ at two different pressures (left: $p = 0.04$; right: $p = 0.004$). Bottom: Histograms of diameter of contact circle between particles (left) and mean first passage time τ_{ij} for random walker to escape initial sphere i to neighboring sphere j through contact circle for $p = 0.00004$ and $N = 10^4$. Lines are Weibull (left) and Frechet (right) distributions for comparison.

intraparticle random walker approach of [7] to a random walk on the contact network of particles with transition rate between nodes/particles on the network $W_{ij} \sim 1/\tau_{ij}$; allowing us to investigate the conductive properties of disorder particulate materials from the interparticle to macroscale in analogy to both solid state approaches [9] and continuum mathematical analysis [11].

In particular, we use the leading order term of the asymptotic analytic formula found in [10,12] for the pair-wise volume-averaged mean first passage time between contacting particles, τ_{ij}. For particle i in contact with j, this MFPT of a walker starting in i hoping to j is $\tau_{ij} \sim V/R_{ij}$, where $V = \frac{\pi}{6}d^3$ is the volume of the particle with diameter d and R_{ij} is the radius of the contact circle formed between the particles. Specifically, the transition rate $W_{ij} = 1/\tau_{ij} = \frac{1}{\pi\tau_0}(R_{ij}/d)$, where $\tau_0 = d^2/24D_0$ is the intraparticle conductive timescale, i.e., the time it takes a random walker to explore a spherical region of size d composed of homogeneous, isotropic material with conductivity D_0. This approach should be contrasted with previous proposals [13] in which the ergodic hypothesis is made in order to approximate the transition rate. There it is assumed that the phase space available for leaving a region is the area of the "port" (particle contact area here); however, the MFPT or escape rate is determined by the fractal repeller for the dynamics in the irregular domain [14]. For intersecting spherical domains, this is apparently dependent upon the radius of the port not its area.

Now, given the local geometry of the contacting, monodisperse spheres and the global topology (connectivity) of the jammed (contact) network, we can write a continuous-time Markov process representing conduction of a quantity $\mathbf{P}$ (suitably normalized to represent the probability of a walker being on node i), on the network

$$\frac{\partial}{\partial t}\mathbf{P}(t) = \mathbf{W}\mathbf{P}(t), \tag{1}$$

$$W_{ij} = \begin{cases} -\frac{12D_0}{\pi d^2}\sqrt{2\delta_{ij}/d} & \text{if } i \neq j, \\ -\sum_{k\neq i} W_{ik} & \text{if } i = j, \end{cases} \tag{2}$$

where we used $R_{ij} \approx \sqrt{\delta_{ij}d/2}$ assuming Hertzian contact for homogeneous elastic materials; $\delta_{ij} = d - ||\mathbf{r}_j - \mathbf{r}_i||$ is the particle overlap from the DEM simulations. The matrix $\mathbf{W}$ is a weighted Graph Laplacian [15] with form $\mathbf{W} = \tilde{\mathbf{D}} - \tilde{\mathbf{A}}$, where $\tilde{\mathbf{D}}$ and $\tilde{\mathbf{A}}$ are the weighted degree [bottom line of Eq. (2)] and adjacency matrices [top line of Eq. (2)], respectively.

The statistics of the elements in the conduction matrix differ from other well-known random matrices (e.g., Gaussian random matrices), in that the matrix is very sparse with a maximum nodal degree 12, due to physical excluded volume constraints from particle interactions, and mean degree $\bar{z} \to 6$ as $p \to 0$. In addition, a Weibull distribution [16] fits the histogram of nonzero contact radii (R_{ij}), i.e., the nonzero elements of the conduction matrix, well (see Fig. 1). A Weibull distribution of contact radii (or transition rates) is also consistent with the Frechet distribution [17] of the per-particle volume-averaged mean first passage times $\bar{t}$ as the two random variates are inversely proportional to each other. Note, the Weibull-like distribution of the transition rates is also consistent with an exponential distribution of the force magnitudes [18] (above the average value) since, if W is distributed according to a Weibull with scale and shape parameters β and k, respectively, then $X = (W/\beta)^k$ is exponentially distributed [19]. All of these facts, of course, are related to the distribution of the overlaps δ_{ij} in the DEM packing simulations. Hence, the fundamental quantities to be accessed experimentally are the distribution of contact radii R_c (or, more generally, the distribution of sizes of contact ellipses in order to assess the local curvature for Hertz contact theory) and the particle volume V_p for the mean first passage time $\sim V_p/R_c$. One final observation regarding the conduction matrix is that, due to conservation laws (e.g., Kirchoff's Laws and energy conservation), the matrix is symmetric positive semidefinite and conserves the total probability such that it satisfies the conditions of the recently named diagonally dominant ensemble [20].

Although Eq. (2) is written for the more physical weighted Laplacian or conduction matrix, an analogous unweighted Laplacian will also be considered below. In this case, the weights on the edges of the graph related to the local geometry of the contacting particles are ignored. Instead, only the topological or connectivity information of the network is retained. The unweighted graph Laplacian is simply $\mathbf{L} = \mathbf{D} - \mathbf{A}$, where $\mathbf{D}$ is the degree matrix (a diagonal matrix whose entries are the vertex degrees of the nodes, i.e., particle coordination number), and $\mathbf{A}$ is the adjacency matrix with entries $a_{ij} = 1$ if particles i and j are in contact and zero otherwise. In the following sections we will analyze both the weighted and unweighted graph Laplacian matrices in terms of their spectra (distribution of eigenvalues) and the statistics of eigenvector components. This will allow us to distinguish between effects due to two types of potential disorder in these systems: geometric and topological. In particular, the following section will show that the long-time scaling of the average decay of a unit impulse is not dependent upon the weighting of the edges of the graph. Physically, this means that the local geometry of the contacts does not determine the bulk, long-time relaxation processes. The scaling is instead set by the network topology as described by the degree and adjacency matrices.

III. SPECTRAL ANALYSIS

The elements of the weighted Laplacian matrix and its eigenvalues are connected to the bulk conduction coefficient of the network (particle pack) via $D_\infty \sim \frac{1}{N}\mathrm{Tr}[\mathbf{W}] = \frac{1}{N}\sum_i^N \lambda_i = \bar{\lambda}$, where λ_i are the eigenvalues of the weighted graph Laplacian or conduction matrix. It can be seen that $\bar{\lambda} = \frac{1}{N}\sum_{i=1}^N 1/\bar{t}_i \sim 1/t^*$. In Fig. 2, we confirm that $D_\infty \sim \bar{\lambda} \sim p^{1/2}$ as expected from [7], where p is the isotropic pressure under which the packs were created. For the unweighted Laplacian $\frac{1}{N}\mathrm{Tr}[\mathbf{L}] - \lambda_c = \bar{\lambda} - z_c \sim p^{1/2}$ as seen in Fig. 2(b), where $z_c = 6$ is the critical coordination number at jamming for frictionless, Hookean spheres [4] which is set by the constraint of global mechanical stability of the packing.

We can further elaborate on the spectral properties of these networks. Figure 3 shows histograms of the eigenvalues of the network Laplacian matrices taken from two particle packs at different pressures. The histograms shown in the top row Fig. 3 contain eigenvalues of the weighted Laplacian matrix

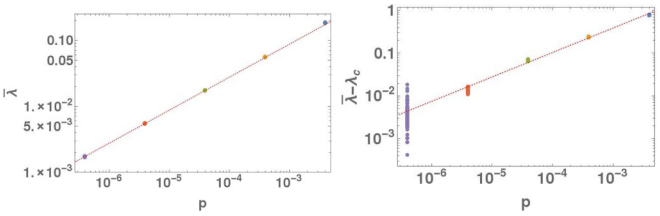

FIG. 2. Variation of mean eigenvalue of weighted (left) and unweighted transition matrix (right) vs. pressure for each $N = 10^4$ configuration at a given pressure. Points represent different pressures; each data point is $\bar{\lambda}$ for a specific configuration (spread of $\bar{\lambda}$ values is small for weighted case). Dashed lines are $\sim p^{1/2}$.

at pressures $p = 0.004$ and $p = 0.00004$, respectively. The histograms shown in the bottom row of Fig. 3 are for eigenvalues of the unweighted Laplacian. Asymmetry can be seen in all the distributions; however, the shift from larger to smaller eigenvalues for lower pressures can be seen most clearly in the unweighted Laplacian particularly when compared to the semicircle distribution (red dashed lines). This is consistent with the fact that $\lambda_{\max} < z_{\max}$ since the network is nonbipartite [15], where $z_{\max} = 12$ is the maximum degree of a node, and $\bar{z} \geqslant 6$ to satisfy constraints on degrees of freedom for global mechanical stability. The distribution of the eigenvalues in the limit $\lambda \to 0$ is of interest as it relates to the macroscopic scaling of relaxation/transport processes on the network. For classical, Euclidean networks/lattices $\rho(\lambda) \sim \lambda^{\nu}$, with $\nu = 1/2$ [21]. Since it is difficult to assess the small λ scaling from the histogram, we instead consider a related quantity—the return probability.

The return probability is a fundamental physical quantity easily determined from the eigenvalue spectrum. It represents the average rate of decay of an initial impulse given to a particle [22]. The particle (ensemble) averaged return probability is [21]

$$\langle P_0(t)\rangle = \langle \delta\mathbf{P}(0)\cdot\delta\mathbf{P}(t)\rangle = \frac{1}{N}\sum_{i=1}^{N}\exp(\lambda_i t), \qquad (3)$$

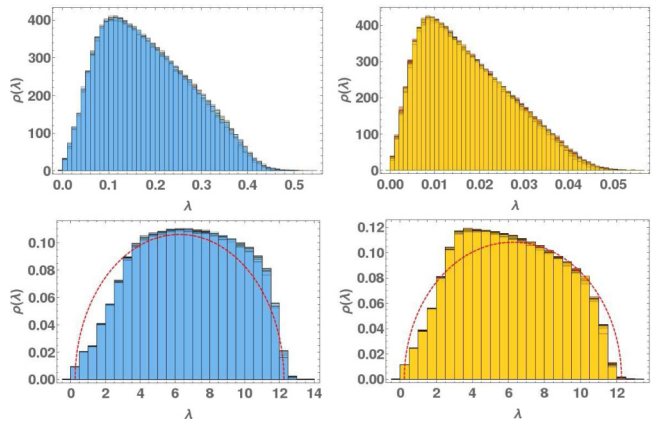

FIG. 3. Top: Histogram of eigenvalues from weighted transition matrix for $p = 0.004$ (left) and $p = 0.00004$ (right). Bottom: Histograms of eigenvalues from unweighted (Graph Laplacian) transition matrix for $p = 0.004$ (left) and $p = 0.00004$) (right); lines are semicircle distribution for comparison. In all cases $N = 10^4$.

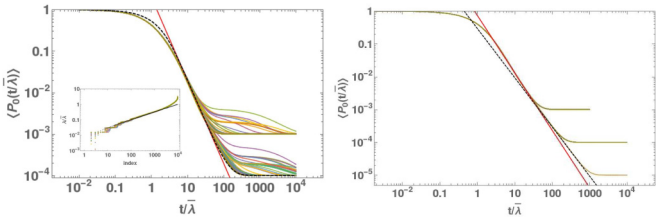

FIG. 4. Return probabilities collapsed by $\bar{\lambda}$ onto Prony series-like master curve (see text). Left: Data for weighted Laplacian for $p = 0.00004$; $N = 10^3$ and 10^4. Note solid line is a power law guide to the eye $\sim t^{-2}$; dashed line is Eq. (4) with $\beta = 2/3$ and $1/\tau = \bar{\lambda}$. Inset shows scaling of λ_k with index k (see text) for all $N = 10^4$ configurations at $p = 0.00004$. Right: Data from unweighted Laplacian for $p = 0.00004$; $N = 10^3$, 10^4, and 10^5; solid and dashed lines are $\sim t^{-2}$ and $t^{-3/2}$, respectively.

where $\delta\mathbf{P}(t) = \mathbf{P}(t) - \mathbf{P}_{\rm eq} = \sum_{i=2}^{N}\exp(\lambda_i t)\mathbf{v}_i$, $\mathbf{P}_{\rm eq} = \mathbf{v}_1$, and $\mathbf{v}_i$ is the orthonormal eigenvector associated with λ_i. For the case of classical diffusion in a homogeneous, 3-D, continuous material the return probability is expected to decay as $t^{-3/2}$ as $t \to \infty$ which is easily seen by considering the solution of the heat equation to a unit impulse applied at the origin of an infinite domain instantaneously at time $t = 0$, and following the decay of temperature at the origin with time [22]. Return probabilities for several networks taken from packings of differing numbers of particles are shown in Fig. 4. Three distinct regions can be seen in these data. The plateau at early times is indicative of the microscopic particle scale where walkers are localized in the initial particle. At longer times the return probability decays in a power-law manner. While it is difficult to extract precisely the scaling in the weighted case due to noise in small eigenvalues, two clear scaling regions appear for larger system sizes in the unweighted case—t^{-2} for intermediate times and $t^{-3/2}$ for long times (red and black dashed line, respectively, in Fig. 4)—which are consistent with the weighted case. Indeed, the data for the unweighted case shown in Fig. 4 are very smooth; collapsing on each other for the various independent configurations and system sizes. Hence, three clear consistent scales appear—microscopic, meso, and macro/homogeneous—across all system sizes and pressures with no clear growing anomalous mesoscale region with decreasing pressure. As can be seen for the different system size data, the crossover from meso to homogeneous scales is of constant size $L \approx 10$ or $N \approx 1000$ for a cubic domain and sets the lower bound for a representative volume element for homogeneous, effective conduction in these systems. Moreover, the similar long-time scaling for the weighted and unweighted cases indicates that the local geometrical disorder (i.e., distribution of contact radii or weights) has little effect on the long-time scaling so long as the system size is large enough $N >\sim 10^3$. Interestingly, the $t^{-3/2}$ scaling gives a "fracton" or "spectral" dimension $d_s = 3$ [21] and indicates the limit of a macroscopic, homogeneous behavior consistent with classical continuum behavior. This is the macroscopic limit where the effective, bulk conductivity D_∞ is a meaningful average or homogenized material property.

To confirm the scaling seen in the return probability, we note that $\langle P_0(t)\rangle$ in Eq. (3) is well described by a Prony

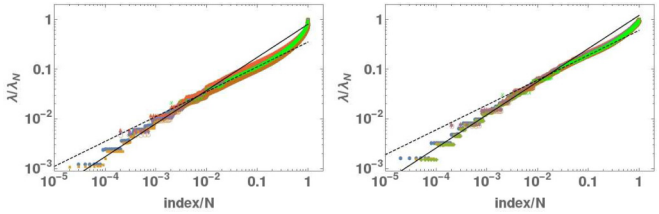

FIG. 5. Collapse of eigenvalues from weighted (left) and unweighted (right) transition matrices for select configurations of $N = 10^3$, 10^4, and 10^5 particles at $p = 0.004$, $p = 0.00004$, and $p = 4 \times 10^{-7}$. Solid and dashed lines are guides to the eye $\sim k^{2/3}$ and $\sim k^{1/2}$, respectively.

series [11]

$$f(t) = \frac{1}{N}\sum_{k=1}^{N} \exp\left(-\left(\frac{k-1}{N}\right)^{\beta} t/\tau\right), \tag{4}$$

with $\beta = 2/3$ and $\overline{\lambda} = 1/\tau$ (see dashed line in Fig. 4 left). Thus, when eigenvalues are sorted from least $\lambda_{k=1}$ to greatest $\lambda_{k=N}$, it is seen that they are distributed according to $\lambda_k \sim (\frac{k-1}{N})^{\frac{2}{3}}$, where $k = 1, 2, \ldots, N$, as in the inset of Fig. 4. If we rescale λ_k by λ_N, all the eigenvalues for all networks from various configurations and pressures collapse onto a single curve as shown in Fig. 5. Again we find $\lambda_k \sim k^{2/3}$ in the limit $k \to 0$ indicating a homogenized macroscale consistent with classical diffusion; although the eigenvalues are more discretely distributed in this limit—they group about discrete levels due to finite system size—no multiplicity of values exists. This fact convolved with the distribution of small contact areas produce the observed noise in the return probability at long times for the weighted case. $\lambda_k \sim k^{2/3}$ is consistent with the classical Weyl result for the Dirichlet eigenvalues of the Laplace operator in 3-D Euclidean space; however, that result applies asymptotically in the other limit $k \to \infty$ [23], the so-called continuum limit, where we find a crossover to an anomalous scaling $\lambda_k \sim k^{1/2}$. In the current case, the continuum limit applies within a given particle at the microscopic scale, whereas at the intermediate mesoscale the discreteness of the material as a collection of densely packed particles is fundamental and not just a numerical approximation for solving a continuous transport equation. We attribute the exact location of this crossover to the disorder in the network (when compared to, e.g., a simple cubic lattice) and the form of the scaling in this limit to the discrete nature of the network. The collapse of all data for all pressures is surprising and suggests the scaling of the crossover location from anomalous to classical with pressure (or volume fraction) is entirely due to the scaling of $\overline{\lambda} = \overline{z}$, while changes in detailed local geometry or coordination number have apparently little effect on the qualitative distribution of eigenvalues. Moreover, changes in system size only serve to extend the domain of the classical distribution of eigenvalues for small eigenvalues in the homogeneous macroscale limit.

IV. EIGENVECTOR STATISTICS

Turning now to the eigenvector statistics, we find similarities to the eigenvector statistics of matrices taken from the Gaussian orthogonal ensemble (GOE) of random matrix theory, but with subtle differences for eigenvectors of the weighted versus the unweighted conductivity matrix. In both cases, eigenvectors associated with large eigenvalues (early times) show significant localization due to network disorder while the distribution of eigenvalue components approaches a common late-time form (in central limit-like fashion) with decreasing eigenvalue consistent with a homogenized macroscale. For the unweighted conductivity matrix, cumulative distribution functions for eigenvector component statistics converge for decreasing eigenvalue to the Porter-Thomas [24] distribution function, $P(x;k) \sim x^{k/2-1}e^{-x/2}$, expected from random matrix theory for a GOE matrix (dashed curve in top panels of Fig. 6, see also lower panels where histograms of the eigenvector components for decreasing λ—left to right—are compared to a Gaussian distribution).

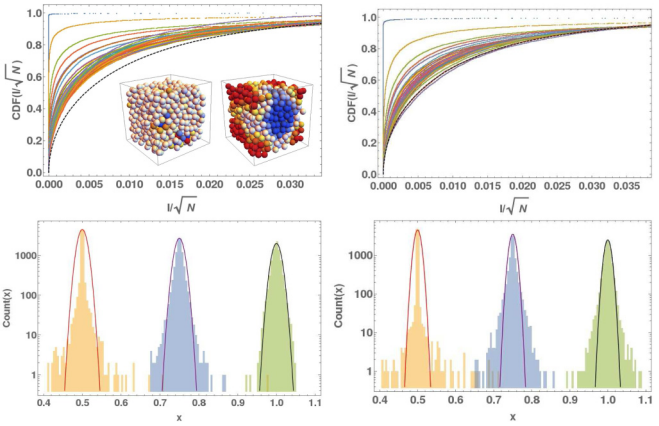

FIG. 6. Top: CDFs of eigenvector components of various eigenvectors associated with decreasing eigenvalue; black dashed lines are CDF for Porter-Thomas distribution. Left: Weighted case for $p = 0.00004$ and $N = 10000$. Inset: Particles colored coded $[-1, 1]$ by contribution to eigenvector for vectors associated with large (left) and small (right) eigenvalues for $N = 1000$ pack. Right: Unweighted case. Bottom: Histograms of eigenvector components compared to Gaussian (solid lines) for various eigenvectors of increasing eigenvalue (shifted for clarity); same p and N as above. Left: Unweighted case. Right: Weighted case.

The Porter-Thomas distribution is known to statisticians as the chi-squared distribution which is the distribution of a random variable that is itself a sum of the squares of k independent Gaussian distributed random variables. Hence, in the unweighted case, the distribution of eigenvector components within a given eigenvector, at least for eigenvectors associated with smaller eigenvalues but above the homogeneous limit ($\lambda = 0$), appear to follow near-Gaussian i.i.d. statistics and are fully delocalized. However, for the statistics of eigenvectors of the weighted conductivity matrix, the quantitative details (see Fig. 6) show that the Porter-Thomas distribution for a single, as this is a scalar problem, independent Gaussian distributed random variable does not quite fit the statistics of the eigenvectors; indicating that the statistics of each particle's contribution to the eigenvector are either not Gaussian, or not independent, or both. We interpret this difference to be a result of the convolution of the random weights (dependent on the distribution of forces in the jammed pack resulting for

the isotropic compression protocol) shown in Fig. 1 with the disordered topology of the network given by the unweighted graph Laplacian shown in Fig. 6. We attribute the early-time localization to the discreteness and inhomogeneity of the network—the distribution of vertex degree or particle coordination number (i.e., topological disorder); while at late times the heavy tails of the eigenvector component distributions lead to an anomalous, increased (as compared to classical Gaussian behavior) influence of a given node/particle to the response of the network/pack and is related to the disorder in the weights (i.e., local geometry of particle contacts) or mean first passage times between pairs of particles. Physically this may imply that while the temporal response of the pack as seen via the distribution of eigenvalues may support a macroscale limit described by an effective, bulk conductivity in an standard fashion, the spatial response indicated by the eigenvector statistics may lead to something other than the classical Gaussian propagator for conduction in these discrete materials. Additional analysis is called for on this point.

V. CONCLUSION

In summary, two structure-property features characterize these "jammed" networks. First, there is a well-described scaling of the mean coordination number or eigenvalue with pressure (volume fraction) ($\overline{\lambda} - \lambda_c \sim p^{1/2}$ for the unweighted and $\overline{\lambda} \sim p^{1/2}$ for the weighted case because the overlaps go to zero with decreasing pressure while the coordination number approaches a constant), which controls the bulk conductive properties of the particle pack. Second, there is inhomogeneity due to (topological) disorder in the coordination number yielding variability in the contribution of a given particle to the bulk transport, i.e., its centrality [25], which also manifests in localized eigenvectors associated with large eigenvalues (early times) for both the weighted and unweighted cases. Also, disorder in the weights on the network due to local geometry variations leads to anomalous eigenvector statistics for the weighted case. Additionally, early time is when the transport is "subdiffusive" (anomalous t^{-2} scaling of return time) due to the discreteness of the network. Inhomogeneity and its concomitant localization as well as heavy-tailed statistics of nodal contributions to eigenvectors, then, could both contribute to a sensitivity of these networks to potential nonlinearities (e.g., breaking contacts or initiating chemistry). This latter point relates to the performance of devices comprised of particulate materials.

As noted in the Introduction, questions about the relationship between the random structure of particulate materials, the forming, or manufacturing processes that determine this structure and the bulk properties related to the performance of these materials are intimately related. As demonstrated here, statistical physics models have an important role to play in advancing the state of the art in this area. This is all the more important as issues of optimal performance and prediction and control of manufacturing processes to ensure efficient energy use and improved yield of robust, reliable devices are critical to resolving intersecting safety and environmental challenges.

ACKNOWLEDGMENTS

This work was performed, in part, at the Center for Integrated Nanotechnologies, an Office of Science User Facility operated for the U.S. Department of Energy (DOE) Office of Science. It was also supported by the Laboratory Directed Research and Development program at Sandia National Laboratories, a multimission laboratory managed and operated by National Technology and Engineering Solutions of Sandia LLC, a wholly owned subsidiary of Honeywell International Inc. for the U.S. Department of Energy's National Nuclear Security Administration under Contract No. DE-NA0003525.

[1] D. Ben-Avraham and S. Havlin, *Diffusion and Reactions in Fractals and Disordered Systems*, Vol. 1 (Cambridge University Press Cambridge, England, 2000).
[2] R. Rammal and G. Toulouse, J. Phys. Lett. **44**, 13 (1983).
[3] L. Lovásv, in *Combinatorics, Paul Erdős is eighty*, Bolyai Society mathematical studies No. Vol. 1, edited by P. Erdős, D. Miklós, V. Sós, T. Szőnyi, and B. J. M. Társulat (János Bolyai Mathematical Society, Budapest, Hungary, 1993), pp. 1–46.
[4] C. S. O'Hern, L. E. Silbert, A. J. Liu, and S. R. Nagel, Phys. Rev. E **68**, 011306 (2003).
[5] L. E. Silbert, A. J. Liu, and S. R. Nagel, Phys. Rev. E **79**, 021308 (2009).
[6] L. E. Silbert, Soft Matter **6**, 2918 (2010).
[7] D. S. Bolintineanu, G. S. Grest, J. B. Lechman, and L. E. Silbert, Phys. Rev. Lett. **115**, 088002 (2015).
[8] S. Torquato and I. C. Kim, Appl. Phys. Lett. **55**, 1847 (1989).
[9] J. Haus, G. Parisi, and K. Kehr, Phys. Rep. **150**, 263 (1987).
[10] A. F. Cheviakov, M. J. Ward, and R. Straube, Multiscale Model. Simul. **8**, 836 (2010).
[11] J. Dodziuk, Am. Math. Mon. **88**, 686 (1981).
[12] D. Holcman and Z. Schuss, J. Phys. A: Math. Theor. **41**, 155001 (2008).
[13] J. Machta and S. M. Moore, Phys. Rev. A **32**, 3164 (1985).
[14] P. Gaspard, *Chaos, Scattering and Statistical Mechanics* (Cambridge University Press, Cambridge, England, 1998).
[15] F. Chung, *Spectral Graph Theory*, CBMS Regional Conference Series No. 92 (American Mathematical Society, Providence, RI, 1997).
[16] W. Weibull, J. Appl. Mech.-Trans. ASME **18**, 293 (1951).
[17] E. Gumbel, *Statistics of Extremes* (Columbia University Press, New York, 1958).
[18] D. M. Mueth, H. M. Jaeger, and S. R. Nagel, Phys. Rev. E **57**, 3164 (1998).
[19] N. L. Johnson, S. Kots, and N. Balakrishnan, *Continuous Univariate Distributions*, Wiley Series in Probability and Mathematical Statistics: Applied Probability and Statistics (2nd ed.), Vol. 1 (John Wiley & Sons, New York, 1994).
[20] M. L. Manning and A. J. Liu, Europhys. Lett. **109**, 36002 (2015).
[21] O. Mülken and A. Blumen, Phys. Rev. E **73**, 066117 (2006).
[22] D. Fournier and A. C. Boccara, Physica A **157**, 587 (1989).
[23] H. Weyl, Math. Ann. **71**, 441 (1912).
[24] C. Porter, *Statistical Theories of Spectral Fluctuations* (Academic, New York, 1965).
[25] J. D. Noh and H. Rieger, Phys. Rev. Lett. **92**, 118701 (2004).